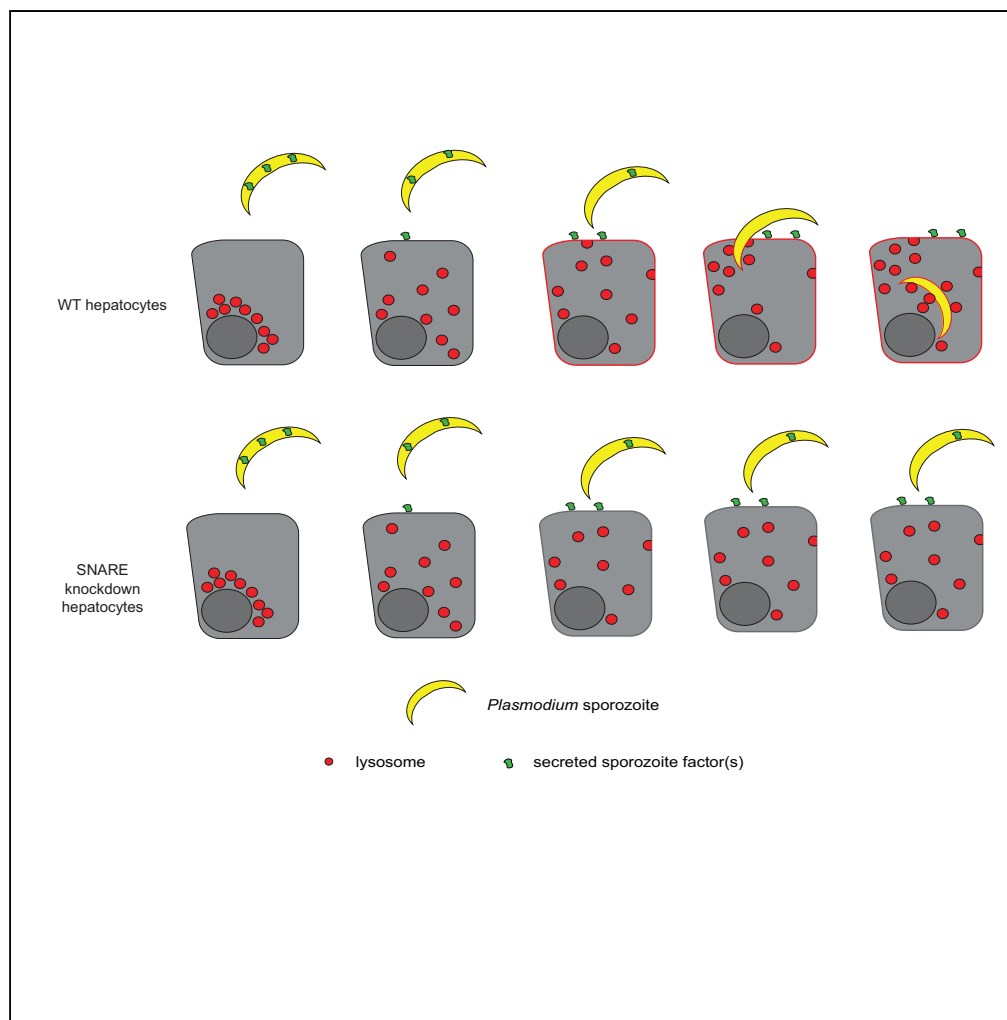


## Article

# Plasmodium Secretion Induces Hepatocyte Lysosome Exocytosis and Promotes Parasite Entry



Kamalakaran  
Vijayan, Igor  
Cestari, Fred D.  
Mast, ..., John D.  
Aitchison,  
Kenneth Stuart,  
Alexis Kaushansky

alexis.kaushansky@  
seattlechildrens.org

## HIGHLIGHTS

*Plasmodium* sporozoites induce host lysosome exocytosis during invasion

Hepatocyte lysosome exocytosis occurs in a SPECT2-independent manner

Inhibition of lysosome-plasma membrane fusion inhibits sporozoite invasion

Secreted parasite factors are sufficient to induce lysosome exocytosis

Vijayan et al., iScience 21,  
603–611  
November 22, 2019 © 2019  
The Author(s).  
[https://doi.org/10.1016/  
j.isci.2019.10.054](https://doi.org/10.1016/j.isci.2019.10.054)

## Article

# *Plasmodium* Secretion Induces Hepatocyte Lysosome Exocytosis and Promotes Parasite Entry

Kamalakkannan Vijayan,<sup>1</sup> Igor Cestari,<sup>1,2</sup> Fred D. Mast,<sup>1,3</sup> Elizabeth K.K. Glennon,<sup>1</sup> Suzanne M. McDermott,<sup>1</sup> Heather S. Kain,<sup>1</sup> Alyssa M. Brokaw,<sup>4</sup> John D. Aitchison,<sup>1,3</sup> Kenneth Stuart,<sup>1,4</sup> and Alexis Kaushansky<sup>1,4,5,\*</sup>

## SUMMARY

The invasion of a suitable host hepatocyte by *Plasmodium* sporozoites is an essential step in malaria infection. We demonstrate that in infected hepatocytes, lysosomes are redistributed away from the nucleus, and surface exposure of lysosome-associated membrane protein 1 (LAMP1) is increased. Lysosome exocytosis in infected cells occurs independently of sporozoite traversal. Instead, a sporozoite-secreted factor is sufficient for the process. Knockdown of SNARE proteins involved in lysosome-plasma membrane fusion reduces lysosome exocytosis and *Plasmodium* infection. In contrast, promoting fusion between the lysosome and plasma membrane dramatically increases infection. Our work demonstrates parallels between *Plasmodium* sporozoite entry of hepatocytes and infection by the excavate pathogen *Trypanosoma cruzi* and raises the question of whether convergent evolution has shaped host cell invasion by divergent pathogens.

## INTRODUCTION

*Plasmodium* parasites, the causative agents of malaria, are transmitted to humans by the bite of infected female *Anopheles* mosquitoes. The sporozoite form of the parasite is deposited into human skin during a blood meal. Sporozoites are motile and rapidly migrate through the skin to enter a capillary, which allows the parasite to travel to the liver. *Plasmodium* sporozoites have the capacity to transmigrate through cells using a process termed cell traversal (CT) (Mota and Rodriguez, 2001). Recent studies have demonstrated that sporozoites can also enter hepatocytes within a transient vacuole, independently of CT, and that parasites that are CT deficient within a transient vacuole associate with lysosomes and are eliminated (Risco-Castillo et al., 2015). In contrast, productive invasion occurs when sporozoites invade a hepatocyte, form a parasitophorous vacuole (PV), and develop into a liver stage (LS) schizont, from which merozoites are released into the bloodstream and invade erythrocytes. The secretion of a multitude of sporozoite factors are released during motility, CT, and invasion, yet a precise role for most secreted factors remains undefined.

Membrane vesicle trafficking is fundamental to eukaryotic life and plays a regulatory role in nearly all cellular activities. Many intracellular pathogens target and subvert these trafficking events for their own benefit (Alix et al., 2011; Asrat et al., 2014). Previous work has demonstrated that the *Plasmodium* liver stage PV membrane co-localizes with late endosomes (Petersen et al., 2017), lysosomes (Lopes da Silva et al., 2012; Niklaus et al., 2019; Prado et al., 2015; Risco-Castillo et al., 2015), and autophagic vesicles (Prado et al., 2015; Real et al., 2018; Wacker et al., 2017). Although these studies have suggested that the vesicle association is gradually lost over the course of liver stage infection (Niklaus et al., 2019; Prado et al., 2015; Risco-Castillo et al., 2015), when this association is initiated during *Plasmodium* life cycle progression remains unknown, and none of these studies have evaluated infection prior to 3 h post-entry. Moreover, the role of host vesicular trafficking processes in sporozoite entry of hepatocytes has not been explored.

## RESULTS AND DISCUSSION

## *Plasmodium* Sporozoites Co-localize with LAMP1-Positive Vesicles

We quantitatively surveyed the extent of co-localization between the parasite and five markers of endocytic compartments. Freshly isolated *Plasmodium yoelii* sporozoites were added to Hepa1-6 cells. After 90 min, cells were fixed, stained, and visualized by 3D fluorescence deconvolution microscopy. We used antibodies against early endosome antigen 1 (EEA1) and Ras-related protein 5 (Rab5) to mark early endosomes, Rab7a to mark late endosomes (LE), Rab11a to mark recycling endosomes, and lysosome-associated membrane

<sup>1</sup>Center for Global Infectious Disease Research, Seattle Children's Research Institute, 307 Westlake Avenue, N. Suite 500, Seattle, WA 98109, USA

<sup>2</sup>Institute of Parasitology, McGill University, Ste Anne de Bellevue, QC H9X 3V9, Canada

<sup>3</sup>Institute for Systems Biology, 401 Terry Avenue, N, Seattle, WA 98109, USA

<sup>4</sup>Department of Global Health, University of Washington, Harris Hydraulics Laboratory Box 357965, Seattle, WA 98195-7965, USA

<sup>5</sup>Lead Contact

\*Correspondence: alexis.kaushansky@seattlechildrens.org

<https://doi.org/10.1016/j.isci.2019.10.054>



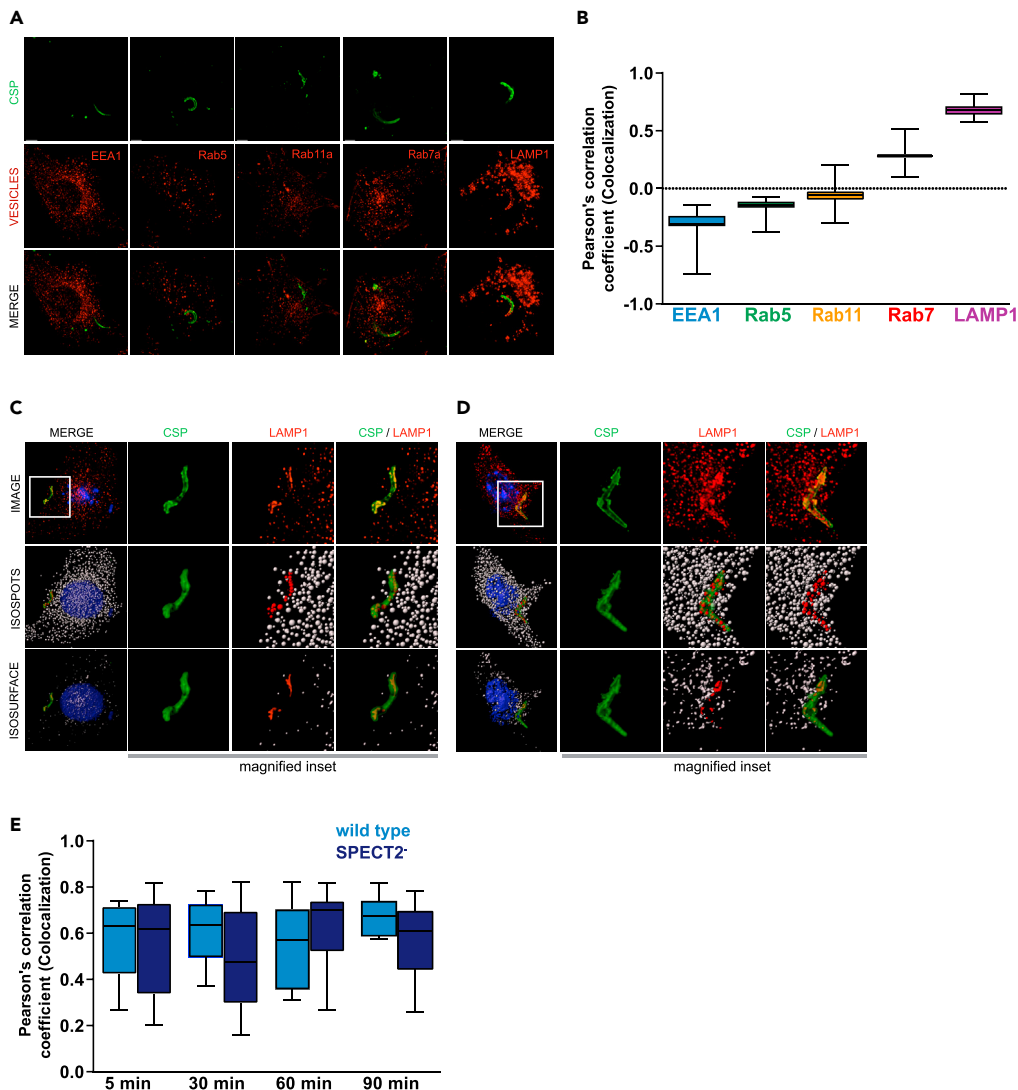


**Figure 1. Plasmodium Sporozoites Co-localize with LAMP1-Positive Vesicles**

(A) Hepa1-6 cells were infected with *P. yoelii* sporozoites for 90 min and processed for fluorescence microscopy using antibodies to EEA1, Rab5a, Rab11, Rab7a, and LAMP1 (red) and PyCSP (green). Scale bar represents 5  $\mu$ m.

(B) Pearson's correlation coefficients were calculated for each endocytic vesicle channel with the sporozoite CSP channel of 25 different microscopic fields from three independent experiments. Hepa1-6 cells were infected with *P. yoelii* sporozoites for 5 min (C) and 30 min (D) and processed for fluorescence microscopy using DAPI (blue) for DNA, phalloidin (white) for actin visualization, antibodies to LAMP1 (red) for LE/lysosomes, and CSP (green) for parasites. Isospot rendering for LE/lysosomes and isosurface rendering for LE/lysosomes, parasites, host cell nucleus, and plasma membrane are shown. Red isospots represent LAMP1-positive structures co-localized with CSP. Magnified inset is 15  $\mu$ m  $\times$  15  $\mu$ m.

(E) Hepa1-6 cells were infected with wild type or SPECT2<sup>-</sup> *P. yoelii* sporozoites and fixed after 5, 30, 60, and 90 min. Intensity-based colocalization was performed on at least 25 parasites per time point and Pearson's correlation coefficients were calculated. Box and whiskers plot depict mean  $\pm$  SD of three independent experiments.

protein 1 (LAMP1) to mark LE/lysosomes. Sporozoites were labeled with an antibody against circumsporozoite protein (CSP) (Figure 1A). Intensity-based co-localization was used (Bolte and Cordelières, 2006) to evaluate the extent of overlap between CSP and staining for each vesicular compartment (Figures 1A and 1B). The Pearson's correlation coefficient between CSP and LAMP1 was  $\sim$ 0.6, but staining did not significantly overlap between CSP and EEA1, Rab5, Rab7a, or Rab11a (Figures 1A and 1B). These data are consistent with earlier observations (Lopes da Silva et al., 2012; Petersen et al., 2017).

We next assessed the kinetics of co-localization between sporozoites and LAMP1. Hepa1-6 cells were infected with *P. yoelii* sporozoites and fixed after 5 (Figure 1C), 30 (1D), 60, or 90 min (1E). LAMP1 structures that co-localized with CSP were observed as early as 5 min and were elongated in the infected cells (Figure 1C). These elongated LAMP1 structures were not observed in bystander or unexposed cells. Thus, the association between LAMP1-positive LE/lysosomes and sporozoites occurs during or very soon after infection and is maintained. We observed a very similar association between LAMP1 and CSP in the CT-deficient parasite, *PySPECT2*<sup>-</sup> (Ishino et al., 2004) (Figures 1E, S1A, and S1B). Our data are consistent with the hypothesis that lysosomes interact with the sporozoite during or very soon after entry, independently of CT. Since *PySPECT2*<sup>-</sup> parasites cannot egress from the transient vacuole, these data do not distinguish between productive and non-productive entry.

### Sporozoite Entry Is Associated with LE/Lysosome Redistribution

Lysosomes are typically located in juxtannuclear regions of the cell under basal conditions but can be redistributed under times of stress or during infection (Yokota et al., 1989). To evaluate lysosome localization during *Plasmodium* infection, we infected Hepa1-6 cells with *P. yoelii* sporozoites and fixed after 30 or 90 min (Figure 2A). To assess the quantity and localization of lysosomes within infected and uninfected cells we defined LE/lysosomes as LAMP1-positive structures between 0.25 and 1  $\mu\text{m}$  in diameter, corresponding to the typical size of LE/lysosomes within the mammalian cell. Hepa1-6 cells contained an average of  $\sim$ 450 LAMP1-positive structures, similar to measurements obtained by other groups (Cortez et al., 2016). We defined perinuclear lysosomes as LAMP1-positive structures that were within a region surrounding the nucleus, delineated by extrapolating the DAPI signal (Cortez et al., 2016). In unexposed or mock-treated samples containing material from the salivary glands of uninfected mosquitoes,  $\sim$ 85% of LE/lysosomes were perinuclear (Figure 2A). In infected cells, lysosomes were slightly higher in number (Figure 2B) and significantly less perinuclear (Figure 2C). Interestingly, bystander cells, which were defined as being immediately proximate to the infected cell, also exhibited an increase in lysosome numbers and redistribution (Figures 2B and 2C).

To assess the fate of redistributed lysosomes, we asked if there was evidence of LAMP1 positive-vesicle fusion with the hepatocyte plasma membrane in infected cells. We infected Hepa1-6 cells with *P. yoelii* sporozoites and evaluated total and surface-exposed LAMP1 (sLAMP1) by flow cytometry (Figure 2D) and immunofluorescence microscopy (Figure S2A). Both LAMP1 and sLAMP1 were elevated in infected cells compared with exposed uninfected and unexposed control cells (Figures 2D and 2E). Interestingly, little impact on sLAMP1, if any, was observed in uninfected cells, despite our earlier observation that lysosomes redistribute in these cells. These data suggest that lysosomes traffic away from the nucleus in infected and neighboring cells but undergo exocytosis only in infected cells. Although we observed an increase in the total number of lysosomes in bystander cells using microscopy-based methodology, we did not observe an increase in total LAMP1 when it was evaluated by flow cytometry on uninfected cells within infected cultures. This difference might originate from the lack of spatial information that can be resolved in flow cytometry experiments. Alternatively, the ability to quantify LAMP1-positive vesicles may be greater using microscopy-based methodology, which could result in our inability to distinguish the modest difference in total LAMP1 levels between bystander and uninfected cells. We observed a similar pattern of lysosome redistribution (Figures S2B–S2D) and elevated levels of sLAMP1 (Figures S3A and S3B) when we infected with *PySPECT2*<sup>-</sup>. Together, these data suggest that lysosome trafficking and exocytosis are altered in infected hepatocytes, independently of CT.

The PV membrane (PVM) is critical for liver-stage development. Soon after productive infection, parasite factors, including upregulated in infectious sporozoites 4 (UIS4), are translated and trafficked to the PVM (Matuschewski et al., 2002). We infected Hepa1-6 cells with wild-type *P. yoelii* sporozoites and fixed samples 3 h after infection. LS parasites with an intact PVM were distinguished by positive CSP and UIS4 staining, and LS parasites positive for CSP but negative for UIS4 were defined as unsuccessful invasion events. We observed co-localization of LAMP1 with parasite markers in both cases (Figure S3C), suggesting that lysosomal contents are associated with intracellular parasites, independently of the status of their PVM.

### The Role of Lysosome Exocytosis Varies across Species of Intracellular Parasites

Lysosomes have been previously demonstrated to play a role in *Trypanosoma cruzi* host cell entry (Tardieux et al., 1992). Specifically, a portion of *T. cruzi* parasites utilize a lysosome-mediated event to enter the host cell (Hissa et al., 2012; Tardieux et al., 1992). In contrast, *Toxoplasma gondii*, an apicomplexan parasite

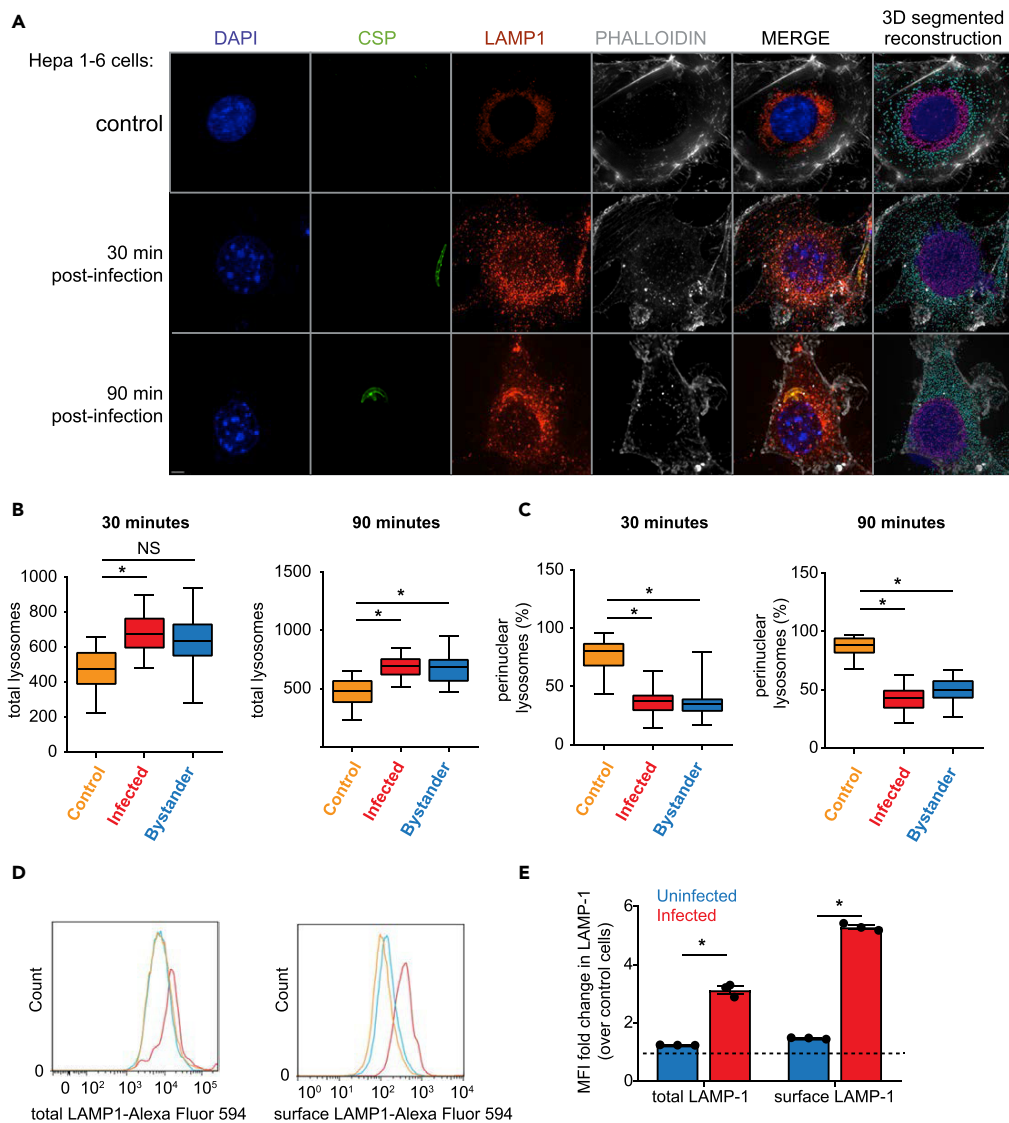


**Figure 2. Sporozoite Entry Is Associated with LE/lysosome Redistribution**

(A) Hepa1-6 cells were infected with *P. yoelii* sporozoites and fixed after 30 or 90 min. DNA was visualized with DAPI (blue), actin with phalloidin (white), LE/Lysosomes with anti-LAMP1 (red), and parasites with anti-CSP (green). Images are maximum intensity projections of the 3D dataset. Scale bar represents 5  $\mu$ m. The isospots corresponding to lysosomes away from the nucleus are cyan while perinuclear lysosomes are shown in magenta.

(B and C) Values represented in box and whiskers plots correspond to lysosomes from total and perinuclear area represented as mean  $\pm$  SD of 25 different microscopic fields from three independent experiments. \* $p < 0.001$ .

(D) Hepa1-6 cells were infected with *P. yoelii* sporozoites for 90 min and analyzed by flow cytometry using antibodies specific to LAMP1 and CSP. The histogram depicts the distribution of total and surface LAMP1 from infected, uninfected, and unexposed control cells from one representative experiment.

(E) Total and surface LAMP1 levels were compared between uninfected and infected cells as a fold change over control cells. The bar graph depicts the mean  $\pm$  the SD of three independent experiments. \* $p < 0.001$ .

closely related to *Plasmodium*, sequesters host lysosomes to the vacuolar space (Coppens et al., 2006) but is not thought to use lysosomes to facilitate host cell entry. To elucidate how the invasion of *Plasmodium* parasites is compared with these two disparate systems, we infected Hepa1-6 cells with *P. yoelii* sporozoites, *T. gondii* tachyzoites, or *T. cruzi* trypomastigotes and assessed infection and sLAMP1 by flow cytometry after 90 min. Cells infected with *P. yoelii* or *T. cruzi*, but not *T. gondii*, exhibited increased sLAMP1 (Figures 3A and 3B).

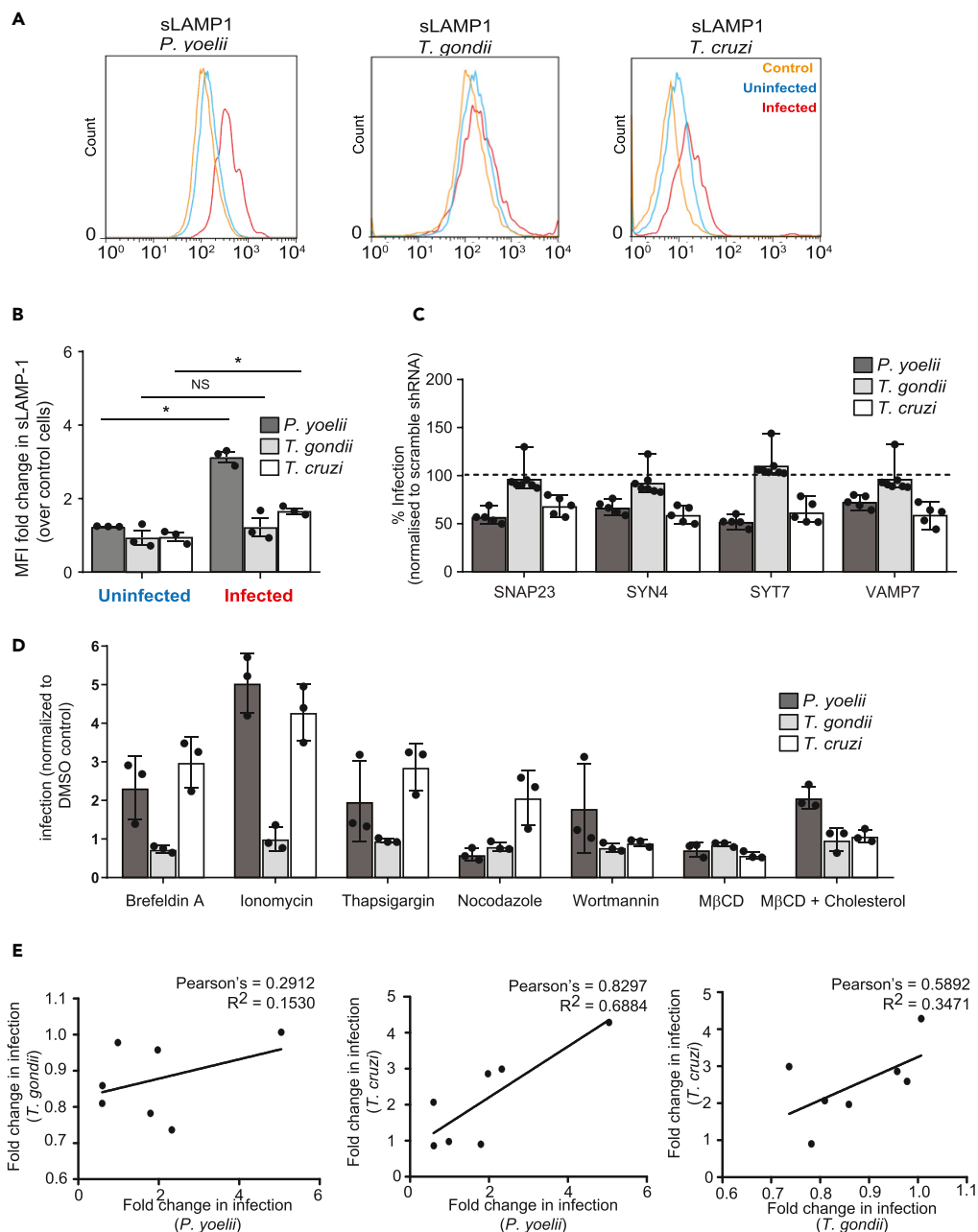


**Figure 3. The Role of Lysosome Exocytosis Varies across Species Of Intracellular Parasites**

(A and B) Hepa1-6 cells were infected with *P. yoelii* sporozoites, *T. gondii* tachyzoites or *T. cruzi* trypomastigotes for 90 min and analyzed by flow cytometry. The histogram shows surface LAMP1 from infected, uninfected, and unexposed control cells. Surface LAMP1 is expressed as fold change over uninfected cells. The bar graph displays the mean  $\pm$  SD of three independent experiments. \* $p < 0.001$ .

(C) Hepa1-6 cells were transduced with shRNA lentiviruses against SNAP23, SYN4, SYT7, VAMP7, or a scrambled control and challenged with *P. yoelii* sporozoites, *T. gondii* tachyzoites, or *T. cruzi* trypomastigotes for 90 min. The bar graph displays the infection rate after knockdown of each transcript of interest normalized to scramble shRNA cells, indicated by dashed line ( $n = 5$  for *Plasmodium* and *Trypanosoma*;  $n = 7$  for *Toxoplasma* infection; mean  $\pm$  SD).

(D) Hepa1-6 cells were incubated with or without the indicated compound for 15 min, washed, and then infected with the indicated parasite for 90 min. The bar graph represents mean  $\pm$  SD of three independent experiments.

(E) Pearson's correlation coefficients were calculated from the data in (D) for each pairwise combination of infections.

Fusion between lysosomes and the plasma membrane is mediated by the SNARE complex, which includes synaptotagmin VII (SYT7), syntaxin 4 (SYN4), vesicle associate membrane protein 7 (VAMP7), and synaptosomal-associated protein 23 (SNAP23) (Rao et al., 2004). We knocked down each factor in Hepa1-6 cells using lentivirus-encoded shRNAs and observed decreased levels of transcript (Figure S4A) and reduced sLAMP1 (Figure S4B) (Rao et al., 2004). We then infected each knockdown line with *T. gondii*, *P. yoelii*, or *T. cruzi* parasites. Knockdown of each member of the SNARE complex significantly reduced *P. yoelii* and *T. cruzi* infections, but not *T. gondii* infection (Figure 3C), and did not reduce the viability of infected cells (Figure S4C).

Genetic knockdowns can sometimes lead to compensatory changes that produce off-target effects. To partially circumvent this, we evaluated the impact of a range of small molecules that modulate lysosome exocytosis (Table S1). We treated Hepa1-6 cells with each compound for 15 min, washed the cells, and then infected with *P. yoelii* sporozoites, *T. gondii* tachyzoites, or *T. cruzi* trypomastigotes for 90 min. Molecules that increase lysosome exocytosis or redistribution (ionomycin, thapsigargin, brefeldin A; Table S1 and Figure S4C) significantly increased *P. yoelii* and *T. cruzi* infection (Figure 3D). In contrast, pretreatment with M $\beta$ CD, which has been previously shown to reduce surface LAMP1 levels by disrupting lipid rafts, reduced our readout of sLAMP1 (Figure S4D) and diminished *P. yoelii* and *T. cruzi* infections (Figure 3D). Levels of sLAMP1 and infection returned to baseline when cholesterol was added, restoring lipid raft formation. No inhibitors substantially altered *T. gondii* infection (Figure 3D). Overall, changes in *P. yoelii* and *T. cruzi* infections were tightly correlated (Pearson Correlation Coefficient, 0.8297) (Figure 3E), whereas other pairwise comparisons were less correlated. Our data suggest that *T. cruzi* and *P. yoelii*, but not *T. gondii*, rely on a lysosome-mediated mechanism to enter the host cell. The extent of these parallels, and ways in which the entry strategies diverge, remains an important area for further investigation.

### Secreted Sporozoite Factor(s) Contribute to Lysosome Redistribution during Invasion

Lysosome exocytosis is induced by the soluble *T. cruzi* factor Tcgp82 (Cortez et al., 2016). To assess if a parallel process occurs during *Plasmodium* entry, we treated sporozoites with FBS to induce secretion and then collected supernatants. We exposed Hepa1-6 cells to this sporozoite-derived, secretion-enriched supernatant at different sporozoite:hepatocyte ratios for 90 min. Cells were monitored for lysosome redistribution by 3D fluorescence microscopy (Figures 4A, 4B, S5A) and sLAMP1 by flow cytometry (Figure 4C). Treating cells with even low quantities of secretion-enriched supernatant, but not heat-inactivated supernatant, promoted lysosome redistribution (Figure 4B), and sLAMP1 was induced in a dose-dependent manner (Figures 4C and S5B). Therefore, sporozoite-induced lysosome redistribution is impacted by different factors or the same factors at different levels than lysosome exocytosis. These results are consistent with a model where two separate secretion-mediated events induce hepatocyte lysosome redistribution and lysosome exocytosis (Figure 4D). Taken together, our data suggest a role for lysosome exocytosis in hepatocyte entry of sporozoites, independently of CT or the presence of the PVM.

A growing collection of evidence suggests that parasites that differ only slightly in genetic makeup can exhibit drastically altered host cell tropism. For example, *Plasmodium* species rely differentially on host proteins CD81 and SRB1 for entry (Manzoni et al., 2017; Risco-Castillo et al., 2014; Silvie et al., 2003), and this relationship cannot be predicted by evolutionary similarity alone (Frech and Chen, 2011). Here, we demonstrate that lysosome-related alterations impact *P. yoelii* and *T. cruzi* infections similarly but have no effect on the apicomplexan parasite, *T. gondii*. These observations raise the question of how quickly pathogens can evolve host cell tropism and whether the similarities we observe are sculpted by convergent evolution. Systematic investigation into mechanisms of host cell invasion across many pathogens with well-defined evolutionary relationships, will allow us to obtain a better understanding of the major influences that shape host cell engagement over evolutionary time.

### Limitations of the Study

In this study, we addressed the role of lysosome exocytosis during *Plasmodium* liver stage infection. Although we systematically explored this process using temporally resolved immunofluorescence imaging, our work does not definitively demonstrate that lysosome exocytosis occurs at the moment of infection. Subsequent work that utilizes live cell imaging could add temporal detail to our findings.

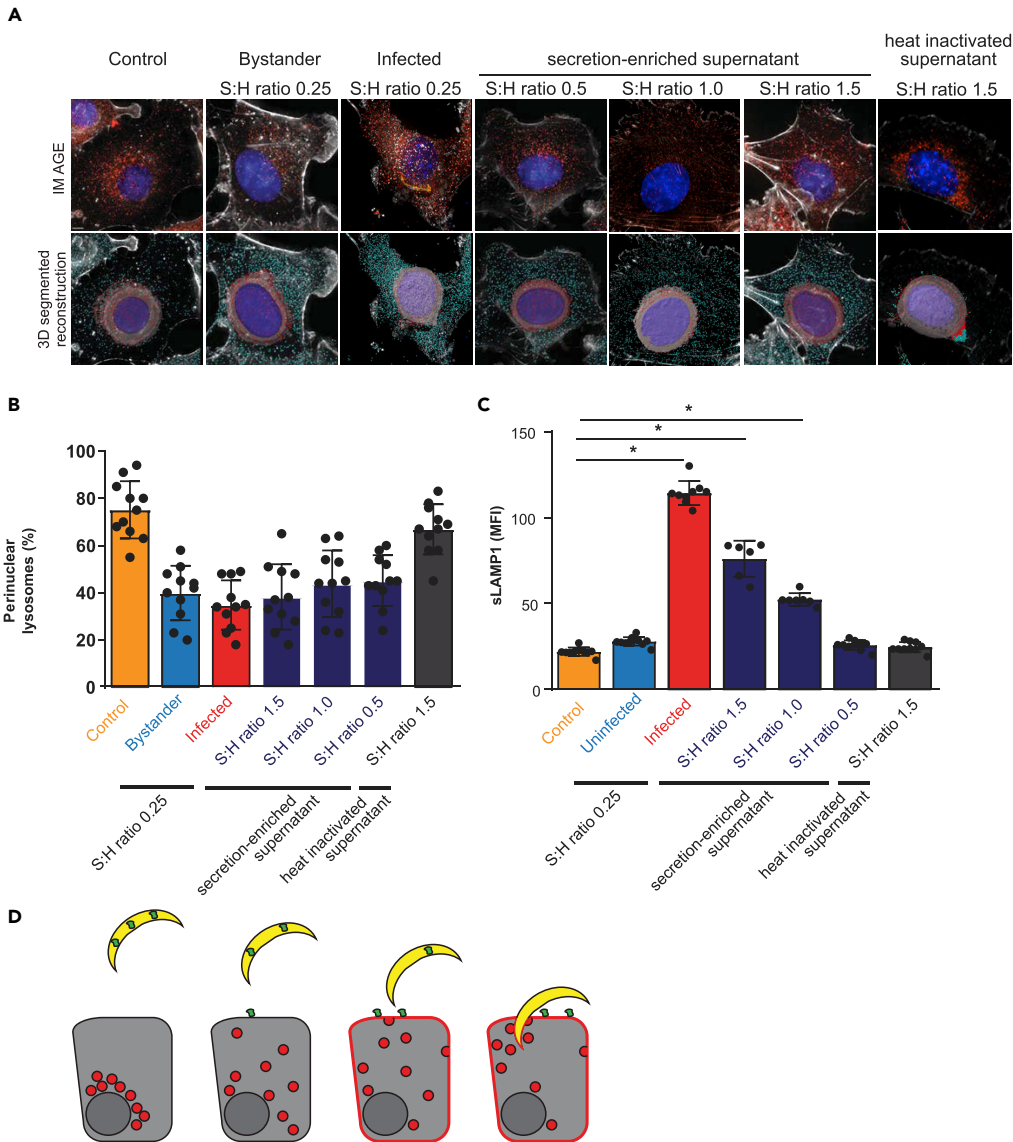


**Figure 4. Secreted Sporozoite Factor(s) Contribute to Lysosome Redistribution during Invasion**

(A) Hepa1-6 cells were infected with *P. yoelii* sporozoites or treated with sporozoite secretion-enriched supernatants at different sporozoite:hepatocyte (S:H) ratios. After 90 min, cells were processed using DAPI (blue) for DNA, phalloidin (white) for actin visualization, antibodies to LAMP1 (red) for LE/lysosomes, and CSP (green) for parasites and displayed as maximum intensity projections. Scale bar represents 5  $\mu$ m. The isospots corresponding to lysosomes away from the nucleus and perinuclear lysosomes were depicted in cyan and magenta, respectively.

(B) Values represented in bar graphs correspond to percentage of perinuclear lysosomes identified in (A). Data represent the mean  $\pm$  SD of at least 10 different microscopic fields per condition from three independent experiments.

(C) Hepa1-6 cells were infected with *P. yoelii* sporozoites or exposed to sporozoite secretion-enriched supernatants. Surface LAMP1 was analyzed by flow cytometry. Values represent the mean  $\pm$  the SD of three independent experiments. \* $p < 0.001$ .

(D) Model of *Plasmodium* sporozoites promoting lysosome exocytosis. Sporozoites are depicted in yellow, hepatocytes in gray, lysosomes in red, and a *Plasmodium*-derived secreted factor in green.

The functional studies contained within this manuscript are performed using pharmacological inhibitors and shRNA-mediated knockdown, each which, has off-target effects. Moreover, we have performed these experiments using cell lines *in vitro*. These technical limitations represent potential caveats of our study.

Finally, we demonstrate that secreted parasite factor(s) are sufficient to induce hepatocyte lysosome exocytosis. Subsequent work will elucidate the specific effectors of this process.

## METHODS

All methods can be found in the accompanying [Transparent Methods supplemental file](#).

## DATA AND CODE AVAILABILITY

The data supporting the findings of this study are available within the paper and its [Supplemental Information](#).

## SUPPLEMENTAL INFORMATION

Supplemental Information can be found online at <https://doi.org/10.1016/j.isci.2019.10.054>.

## ACKNOWLEDGMENTS

We thank Marilyn Parsons for the RHΔHXGPRT *T. gondii* strain. We thank the Center for Infectious Disease Research/Seattle Children's Research Institute vivarium staff for their work with mice. All work was done according to IACUC procedures and protocols. This work was supported by National Institutes of Health grants R01GM101183 (AK), 1K99/R00AI111785 (AK), R01AI014102 (KS, IC and SM), P41 GM109824. (JDA), T32 Post-Doctoral Fellowship AI07509 (EKKG), a W.M. Keck Foundation award (AK), Science and Engineering Research Board, and INDO-US Science and Technology Forum - Overseas Post-Doctoral Fellowship (KV). FDM is a postdoctoral fellow with the Canadian Institutes of Health Research.

## AUTHOR CONTRIBUTIONS

K.V., E.K.K.G., I.C., S.M., H.S.K., and A.M.B. performed experiments. K.V., I.C., and F.D.M. analyzed data. J.D.A., K.S., and A.K. supervised the research. K.V. and A.K. wrote the paper with input from all other authors.

## DECLARATION OF INTERESTS

The authors declare no competing interests.

Received: May 14, 2019

Revised: October 17, 2019

Accepted: October 24, 2019

Published: November 22, 2019

## REFERENCES

- Alix, E., Mukherjee, S., and Roy, C.R. (2011). Subversion of membrane transport pathways by vacuolar pathogens. *J. Cell Biol.* 195, 943–952.
- Asrat, S., de Jesus, D.A., Hempstead, A.D., Ramabhadran, V., and Isberg, R.R. (2014). Bacterial pathogen manipulation of host membrane trafficking. *Annu. Rev. Cell Dev. Biol.* 30, 79–109.
- Bolte, S., and Cordelières, F.P. (2006). A guided tour into subcellular colocalization analysis in light microscopy. *J. Microsc.* 224, 213–232.
- Coppens, I., Dunn, J.D., Romano, J.D., Pypaert, M., Zhang, H., Boothroyd, J.C., and Joiner, K.A. (2006). *Toxoplasma gondii* sequesters lysosomes from mammalian hosts in the vacuolar space. *Cell* 125, 261–274.
- Cortez, C., Real, F., and Yoshida, N. (2016). Lysosome biogenesis/scattering increases host cell susceptibility to invasion by *Trypanosoma cruzi* metacyclic forms and resistance to tissue culture trypomastigotes. *Cell Microbiol.* 18, 748–760.
- Frech, C., and Chen, N. (2011). Genome comparison of human and non-human malaria parasites reveals species subset-specific genes potentially linked to human disease. *PLoS Comput. Biol.* 7, e1002320.
- Hissa, B., Duarte, J.G., Kelles, L.F., Santos, F.P., del Puerto, H.L., Gazzinelli-Guimaraes, P.H., de Paula, A.M., Agero, U., Mesquita, O.N., Guatimosim, C., et al. (2012). Membrane cholesterol regulates lysosome-plasma membrane fusion events and modulates *Trypanosoma cruzi* invasion of host cells. *PLoS Negl. Trop. Dis.* 6, e1583.
- Ishino, T., Yano, K., Chinzei, Y., and Yuda, M. (2004). Cell-passage activity is required for the malarial parasite to cross the liver sinusoidal cell layer. *PLoS Biol.* 2, E4.
- Lopes da Silva, M., Thieleke-Matos, C., Cabrita-Santos, L., Ramalho, J.S., Wavre-Shapton, S.T., Futter, C.E., Barral, D.C., and Seabra, M.C. (2012). The host endocytic pathway is essential for *Plasmodium berghei* late liver stage development. *Traffic* 13, 1351–1363.
- Manzoni, G., Marinach, C., Topcu, S., Briquet, S., Grand, M., Tolle, M., Gransagne, M., Lescar, J., Andolina, C., Franetich, J.F., et al. (2017). *Plasmodium* P36 determines host cell receptor usage during sporozoite invasion. *Elife* 6, e25903.
- Matuschewski, K., Ross, J., Brown, S.M., Kaiser, K., Nussenzweig, V., and Kappe, S.H. (2002). Infectivity-associated changes in the transcriptional repertoire of the malaria parasite sporozoite stage. *J. Biol. Chem.* 277, 41948–41953.
- Mota, M.M., and Rodriguez, A. (2001). Migration through host cells by apicomplexan parasites. *Microbes Infect.* 3, 1123–1128.
- Niklaus, L., Agop-Nersesian, C., Schmuckli-Maurer, J., Wacker, R., Grunig, V., and Heussler, V.T. (2019). Deciphering host lysosome-mediated

elimination of *Plasmodium berghei* liver stage parasites. *Sci. Rep.* 9, 7967.

Petersen, W., Stenzel, W., Silvie, O., Blanz, J., Saftig, P., Matuschewski, K., and Ingmundson, A. (2017). Sequestration of cholesterol within the host late endocytic pathway restricts liver-stage *Plasmodium* development. *Mol. Biol. Cell* 28, 726–735.

Prado, M., Eickel, N., De Niz, M., Heitmann, A., Agop-Nersesian, C., Wacker, R., Schmuckli-Maurer, J., Caldelari, R., Janse, C.J., Khan, S.M., et al. (2015). Long-term live imaging reveals cytosolic immune responses of host hepatocytes against *Plasmodium* infection and parasite escape mechanisms. *Autophagy* 11, 1561–1579.

Rao, S.K., Huynh, C., Proux-Gillardeaux, V., Galli, T., and Andrews, N.W. (2004). Identification of SNAREs involved in synaptotagmin VII-regulated lysosomal exocytosis. *J. Biol. Chem.* 279, 20471–20479.

Real, E., Rodrigues, L., Cabal, G.G., Enguita, F.J., Mancio-Silva, L., Mello-Vieira, J., Beatty, W., Vera, I.M., Zuzarte-Luis, V., Figueira, T.N., et al. (2018). *Plasmodium* UIS3 sequesters host LC3 to avoid elimination by autophagy in hepatocytes. *Nat. Microbiol.* 3, 17–25.

Risco-Castillo, V., Topcu, S., Marinach, C., Manzoni, G., Bigorgne, A.E., Briquet, S., Baudin, X., Lebrun, M., Dubremetz, J.F., and Silvie, O. (2015). Malaria sporozoites traverse host cells within transient vacuoles. *Cell Host Microbe* 18, 593–603.

Risco-Castillo, V., Topcu, S., Son, O., Briquet, S., Manzoni, G., and Silvie, O. (2014). CD81 is required for rhoptry discharge during host cell invasion by *Plasmodium yoelii* sporozoites. *Cell Microbiol.* 16, 1533–1548.

Silvie, O., Rubinstein, E., Franetich, J.F., Prenant, M., Belnoue, E., Renia, L., Hannoun, L., Eling, W., Levy, S., Boucheix, C., et al. (2003). Hepatocyte

CD81 is required for *Plasmodium falciparum* and *Plasmodium yoelii* sporozoite infectivity. *Nat. Med.* 9, 93–96.

Tardieux, I., Webster, P., Ravesloot, J., Boron, W., Lunn, J.A., Heuser, J.E., and Andrews, N.W. (1992). Lysosome recruitment and fusion are early events required for trypanosome invasion of mammalian cells. *Cell* 71, 1117–1130.

Wacker, R., Eickel, N., Schmuckli-Maurer, J., Annoura, T., Niklaus, L., Khan, S.M., Guan, J.L., and Heussler, V.T. (2017). LC3-association with the parasitophorous vacuole membrane of *Plasmodium berghei* liver stages follows a noncanonical autophagy pathway. *Cell. Microbiol.* 19, 12754.

Yokota, S., Himeno, M., and Kato, K. (1989). Immunocytochemical localization of acid phosphatase in rat liver. *Cell Struct Funct* 14, 163–171.

ISCI, Volume 21

## Supplemental Information

### ***Plasmodium* Secretion Induces Hepatocyte**

### **Lysosome Exocytosis and Promotes Parasite Entry**

**Kamalakaran Vijayan, Igor Cestari, Fred D. Mast, Elizabeth K.K. Glennon, Suzanne M. McDermott, Heather S. Kain, Alyssa M. Brokaw, John D. Aitchison, Kenneth Stuart, and Alexis Kaushansky**

## 1 **Transparent Methods**

### 2 **Cell lines and culture**

3 Hepa1-6 cells were obtained from American Type Culture Collection. Cells were maintained in  
4 DMEM-Complete Medium (Dulbecco's modified eagle medium (Cellgro, Manassas, VA),  
5 supplemented with 10% FBS (Sigma-Aldrich, St. Louis, MO), 10000 IU/ml penicillin, 100 mg/ml  
6 streptomycin (Cellgro), 2.5 mg/ml fungizone (HyClone/Thermo Fisher, Waltham, MA) and 4 mM  
7 L-Glutamine (Cellgro). Cells were split 2-3 times weekly. All experiments were performed using  
8 Hepa1-6 cells that were passaged between 4 and 20 times after purchase from ATCC.

### 9 **Mosquito rearing and sporozoite production**

10 For *P. yoelii* sporozoite production, female 6–8-week-old Swiss Webster mice (Harlan,  
11 Indianapolis, IN) were injected with blood stage *P. yoelii* (17XNL) parasites to begin the growth  
12 cycle. Animal handling was conducted according to the Institutional Animal Care and Use  
13 Committee-approved protocols. *Anopheles stephensi* mosquitoes were allowed to feed on infected  
14 mice after gametocyte exflagellation was observed. Salivary gland sporozoites were isolated using  
15 a standard protocol at day 14 or 15 post-blood meal. The sporozoites were activated with 20% FBS  
16 and spun at 1000 x g to remove debris from salivary gland. Spin sporozoites at 15,000 x g for 4 min  
17 at 4°C to pellet and resuspend in the desired volume of complete medium.

### 18 ***T. gondii* production**

19 *T. gondii* strain RHΔHXGPRT Gra2:GFP, Tub:βgal, a kind gift from Marilyn Parsons (CIDR,  
20 Seattle), was maintained by continual cycling through human foreskin fibroblasts (HFF). For

21 infections, parasites were lysed from HFFs by passing 2× through a 27-gauge needle and then  
22 counted on a hemocytometer.

### 23 ***T. cruzi* production and labeling**

24 Tissue culture-derived trypomastigotes from the *T. cruzi* Cl Brener strain were obtained by weekly  
25 passage in confluent monolayers of Hepa1-6 cells at 37 °C and 5% CO<sub>2</sub>, in DMEM medium  
26 supplemented with 10% FBS. Motile trypomastigotes were obtained from the supernatant and  
27 purified as previously described (Schenkman et al., 1991) and stained with 5(6)-  
28 Carboxyfluorescein diacetate N-succinimidyl ester (Sigma Aldrich) as suggested by  
29 manufacturer's protocol.

### 30 **shRNA-mediated gene knockdown**

31 MISSION shRNA vectors for SNAP23, VAMP7, SYT7 and SYN4 were obtained from Sigma  
32 Aldrich (St. Louis, MO). Non-replicating lentiviral stocks were generated by transfection of  
33 HEK293-FT cells. 4 × 10<sup>6</sup> HEK293-FT cells were plated on poly-L-lysine coated dishes to achieve  
34 70-80% confluency at time of transfection. Approximately 24 h after plating, transfection mixtures  
35 were prepared by mixing 20 µL Polyethylenimine MAX (Polysciences Inc, Warrington, PA)  
36 prepared at 1 mg/ml, together with 4.75 µg of shRNA construct or a scramble shRNA control, 1.5  
37 µg viral envelope plasmid (pCMV-VSV-G), and 3.75 µg viral packaging plasmid (psPax2). After  
38 incubating for 10 min at room temp in DMEM, transfection complexes were added drop-wise to  
39 cells. After overnight incubation, cells were washed to remove transfection mixtures and were fed  
40 with 10 mL fresh media. Lentivirus-containing supernatant was harvested 36 hours later, passed  
41 through 0.45 µm syringe filters, and either used immediately for transduction or stored at -80 °C.

42 To induce knockdown of candidate SNARE proteins, Hepa1-6 cells were transduced with  
43 lentiviral supernatants in 6-well plates at a cell density of  $1 \times 10^6$  per well. At time of plating, cells  
44 were transduced with 1 mL of supernatant in the presence of 0.5  $\mu\text{g/mL}$  polybrene (Sigma Aldrich  
45 St. Louis, MO). In order to select for cells with stable integration of shRNA transgenes, supernatant  
46 was replaced with complete media with the addition of 2  $\mu\text{g/mL}$  puromycin 24 h post-transduction,  
47 and cells were selected for at least 5 days prior to experiments.

#### 48 **Validation and quantification of shRNA mediated knockdown**

49 Total RNA was extracted using TRIzol reagent according to the manufacturer's procedure  
50 (Invitrogen). cDNA synthesis was performed using the Thermo Scientific RevertAid RT Kit  
51 according to the manufacturer's instructions (Thermo Scientific). For quantitative PCR (qPCR) a  
52 standard curve was generated using 1:4 dilutions of a reference cDNA sample for PCR  
53 amplification of all target PCR products using target specific primers (Table S1). The values of  
54 each transcript were normalized to mouse GAPDH. Experimental samples were compared to this  
55 standard curve to give a relative abundance of transcript.

#### 56 **Infection assays**

57  $5 \times 10^5$  Hepa1-6 wild type cells or knockdowns cells were seeded in each well of a 24-well plate  
58 (Corning) and infected with *P. yoelii* sporozoites at a multiplicity of infection (MOI) = 0.25,  
59 *Toxoplasma gondii* tachyzoites (MOI = 0.5) or *Trypanosoma cruzi* trypomastigotes (MOI = 5) for  
60 90 min. For small molecule treatment experiments, Hepa1-6 cells were treated with or without 10  
61  $\mu\text{M}$  ionomycin, 400 nM thapsigargin, 10  $\mu\text{M}$  brefeldin A, 10  $\mu\text{M}$  nocodazole and 5mM methyl- $\beta$ -  
62 cyclodextrin (M $\beta$ CD) for 15 min, washed and infected for 90 min. For cholesterol replenishment,  
63 M $\beta$ CD treated cells were washed and incubated with 1 mM cholesterol for 15 min before parasite

64 addition. Cells were stained with Live/Dead marker after 60 mins of infection as per  
65 manufacturer's instruction (ThermoFischer). After 90 min of infection, cells were harvested with  
66 accutase (Life technologies) and fixed with Cytoperm/Cytofix (BD Biosciences). Cells were  
67 blocked with Perm/Wash (BD Biosciences) + 2% BSA for one hour at room temperature then  
68 stained overnight at 4 °C with primary antibody. Cells were washed three times with PBS then  
69 stained for one hour at room temperature with secondary antibodies. The cells were then washed  
70 and resuspended in PBS + 5 mM EDTA. Infection rate was measured by flow cytometry on an  
71 LSRII (Becton-Dickinson) and analyzed by FlowJo (Tree Star). Surface LAMP-1 levels were  
72 calculated using mean fluorescent intensity of specific population in FlowJo and represented as  
73 fold change between infected and control population.

74 For the evaluation of surface expression of LAMP-1, cells were detached using Accutase (Sigma)  
75 and were incubated with a polyclonal antibody to LAMP1 (DSHB) in medium + 2% BSA for 30  
76 minutes in ice, fixed with 3.7% paraformaldehyde, permeabilized with 0.01% Triton X-100. Cells  
77 were then stained with monoclonal antibody to *P. yoelii* Circumsporozoite protein (CSP)  
78 conjugated to AlexaFluor 488 (Life Technologies) at 1:500, *T. gondii* P30 mouse monoclonal  
79 antibody at 1:1000 (Novus Biologicals). Cells were washed three times with PBS then stained for  
80 one hour at room temperature with secondary antibodies. The cells were washed and suspended in  
81 PBS+5 mM EDTA. Infection rate and surface expression of LAMP1 was measured by flow  
82 cytometry on an LSRII (Becton-Dickinson) and analyzed by FlowJo (Tree Star).

### 83 **3D Fluorescence Microscopy**

84 For imaging experiments, Hepa1-6 cells were plated in 8 well chamber slides (Labtek) and infected  
85 with *P. yoelii* wild type or SPECT2<sup>-</sup> sporozoites. Cells were fixed with 10% formalin (Sigma) at

86 defined timepoints after infection (5, 30, 60, or 90 min), permeabilized with Triton X-100, and  
87 stained with rabbit anti-EEA1 (CST), rabbit anti-Rab5 (CST), rabbit anti-Rab7 (CST), rabbit anti-  
88 Rab11 (CST), rat anti-LAMP1 (DSHB), goat anti-UIS4 (SCIGEN) and mouse anti-CSP  
89 antibodies. Nuclei were stained with DAPI (Vectashield) and AlexaFluor 647-phalloidin (Life  
90 technologies) was used for actin visualization. Images were acquired with a 100× 1.4 NA objective  
91 (Olympus) on a DeltaVision Elite High Resolution Microscope (GE Healthcare Life Sciences).  
92 The sides of each pixel represent  $64.5 \times 64.5$  nm and z-stacks were acquired at 300 nm intervals.  
93 Approximately 20-30 slices were acquired per image stack. For deconvolution, the 3D data sets  
94 were processed to remove noise and reassign blur by an iterative Classic Maximum Likelihood  
95 Estimation widefield algorithm provided by Huygens Professional Software (Scientific Volume  
96 Imaging BV, The Netherlands).

### 97 **Image analysis and quantification**

98 Imaris software (Bitplane) was used to obtain 3D reconstructions of the fluorescence microscopy  
99 image stacks and quantification of lysosomes in x-y-z coordinates. Deconvolved images of  
100 immunostained cells stained with anti-LAMP1 (lysosomes) anti-CSP (sporozoites) and phalloidin  
101 (actin) with DAPI (nucleus) were processed, thresholded and segmented by Imaris software, to  
102 render isospots and isosurfaces from the fluorescence signal (Real and Mortara, 2012). Phalloidin  
103 channel was used for the 3D reconstruction of the cells and only the sporozoites encased inside the  
104 3D phalloidin structure are considered as invaded sporozoites and proceeded further. Isosurfaces  
105 were constructed by extrapolating the DAPI signal to the local minima (Cortez et al., 2016) in  
106 order to define a perinuclear region where lysosomes can be differentially counted. Using a mask  
107 tool, all LAMP1 signal outside this nuclear/perinuclear isosurface was suppressed, allowing  
108 addition of a new LAMP1 fluorescence channel corresponding exclusively to LAMP1 localized

109 in perinuclear area. After image processing, we obtained an unmasked LAMP1 signal  
110 corresponding to total lysosomes and a masked LAMP1 signal localized to the perinuclear region,  
111 corresponding to perinuclear lysosomes. Isospots were constructed based on these two classes of  
112 LAMP1 signal, which allowed the quantification of total and perinuclear lysosomes per cell for  
113 each image-stack. The surface segmentation function of Imaris was used to identify the cell  
114 boundary using phalloidin-signal. Intensity based co-localization was performed by creating  
115 region of interest (ROI) specific to the sporozoite structure in the CSP channel using the Imaris  
116 isosurface module. Pearson's correlation coefficient for co-localization analysis of endocytic  
117 vesicles and CSP was performed in the ROI using the Imaris co-localization module.

#### 118 **Generation of sporozoite supernatant**

119 Salivary gland sporozoites were isolated using standard protocols. Sporozoites incubated with 20%  
120 FBS for 20 min at RT and spun at 13,0000 x g for 4 min at 4 °C. The supernatant is collected and  
121 again spun at 13, 0000 x g for 4 min at 4 °C to ensure the preparation is free of intact sporozoites.  
122 Hepa1-6 cells were exposed to supernatants at different sporozoite to hepatocyte ratio for 90 min.  
123 Cells were washed and subjected to 3D immunofluorescence microscopy or flow cytometry as  
124 described previously.

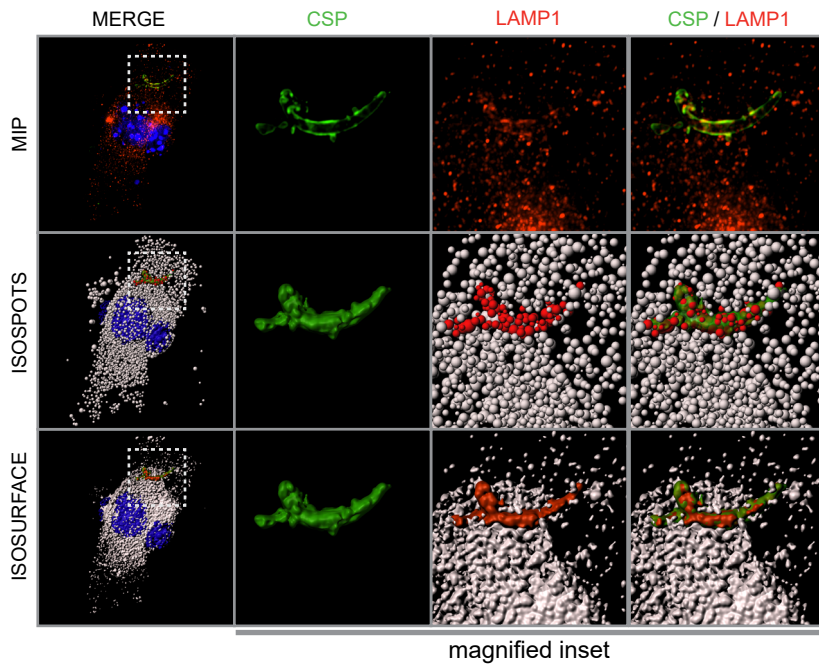
#### 125 **Statistical analysis**

126 p-values were determined in GraphPad Prism 8 software using two tailed end t-test for samples  
127 with unequal variance.

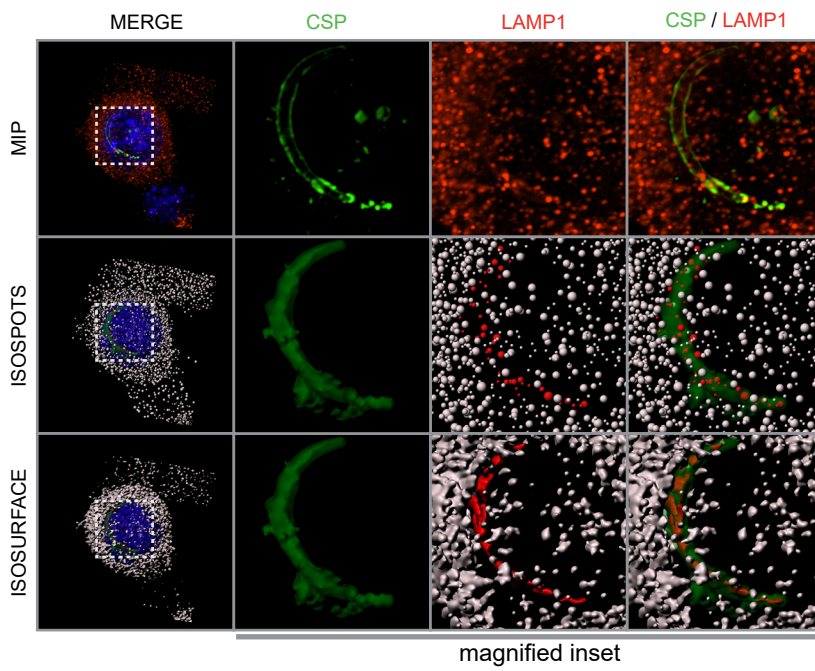
128

129

a



b



130 **Fig. S1. CT deficient or wild type *Plasmodium* sporozoites interacts with lysosomes in similar**  
131 **fashion.** Immunofluorescent microscopy of Hepa1-6 cells infected with SPECT2<sup>-</sup> *P. yoelii*  
132 sporozoites. Infection was assessed after (a) 5 or (b) 30 min and processed for fluorescence  
133 microscopy using DAPI (blue) for DNA, Phalloidin (white) for actin visualization, antibodies to  
134 LAMP1 (red) for LE/lysosomes and CSP (green) for parasites. Isospots for LE/lysosomes and  
135 isosurfaces for LE/lysosomes, parasites, host cell nucleus and plasma membrane were created  
136 using Imaris software and the LE/lysosomes interacting with parasites were identified by detecting  
137 overlap between isospots and the isosurface. Red spots represent LAMP1-positive structures co-  
138 localized with CSP. Magnified inset is 15  $\mu\text{m}$  x 15  $\mu\text{m}$ . Related to Figure 1.

139

140

141

142

143

144

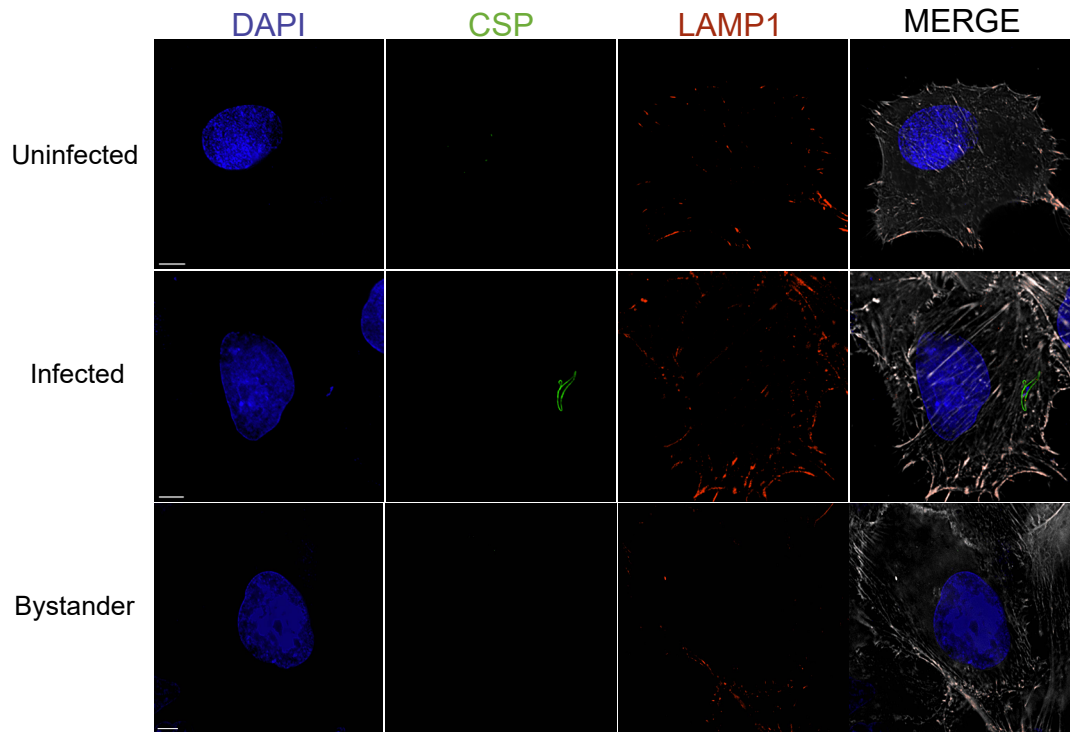
145

146

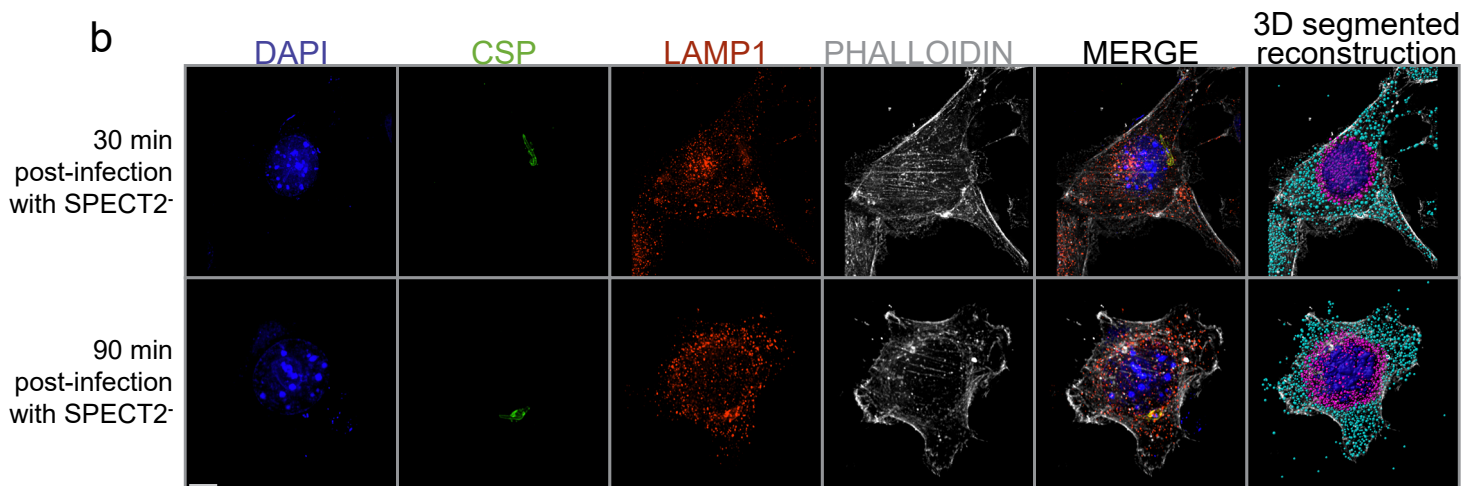
147

148

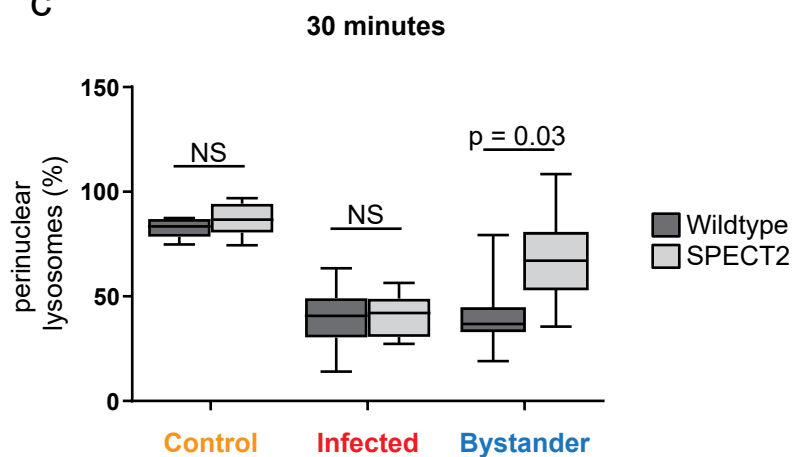
a



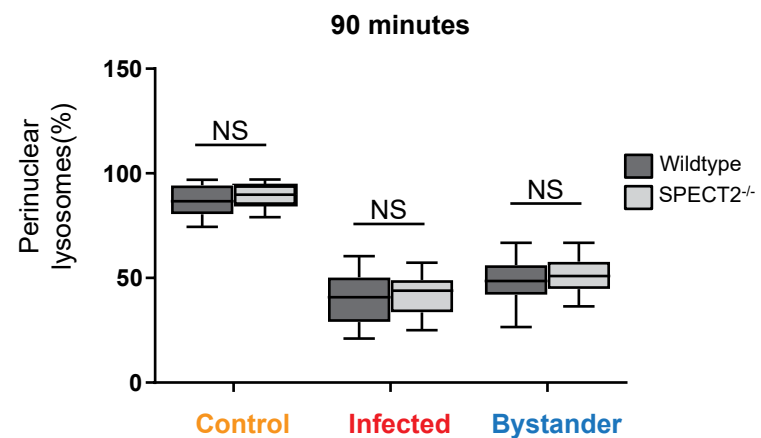
b



c



d



149 **Fig. S2. Sporozoite induced lysosome-plasma membrane fusion is independent of cell**  
150 **traversal. (a)** Hepa1-6 cells were infected with *P. yoelii* sporozoites and fixed after 90 min. Cells  
151 were stained with antibodies to LAMP1 prior to permeabilization and stained with DAPI (blue)  
152 for DNA, phalloidin (white) for actin visualization, antibodies to CSP (green) for parasites and  
153 displayed as maximum intensity projections. Bar = 5  $\mu$ m. **(b)** Hepa1-6 cells were infected with  
154 SPECT2<sup>-</sup> sporozoites and fixed after 30 and 90 min. Cells were processed for 3D fluorescence  
155 microscopy using DAPI (blue) for DNA, phalloidin (white) for actin visualization, antibodies to  
156 LAMP1 (red) for LE/lysosomes and CSP (green) for parasites and displayed as maximum intensity  
157 projections. Scale bar = 5  $\mu$ m. Images were obtained on a Deltavision fluorescence microscope and  
158 processed by Imaris software to construct isosurfaces (nuclei and parasite) and LAMP1-positive  
159 isospots (LE and lysosomes) by predefined algorithms for identification of surfaces and spots.  
160 Perinuclear isosurfaces were created by extrapolating the DAPI signal to define a perinuclear  
161 region where lysosomes could be differentially quantified. The isospots corresponding to total and  
162 perinuclear lysosomes were depicted in cyan and red, respectively. Bar = 5  $\mu$ m. **(c and d)** Values  
163 represented in box and whiskers plot correspond to lysosomes from total and perinuclear area  
164 represented as mean  $\pm$  SD of 25 different microscopic fields from three independent experiments.  
165 Related to Figure 2.

166

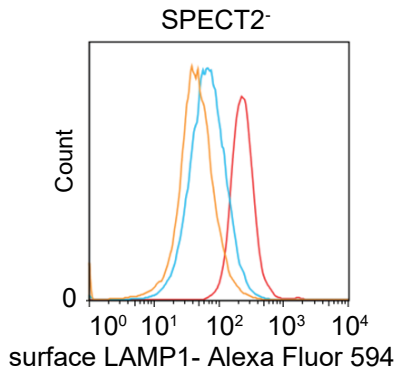
167

168

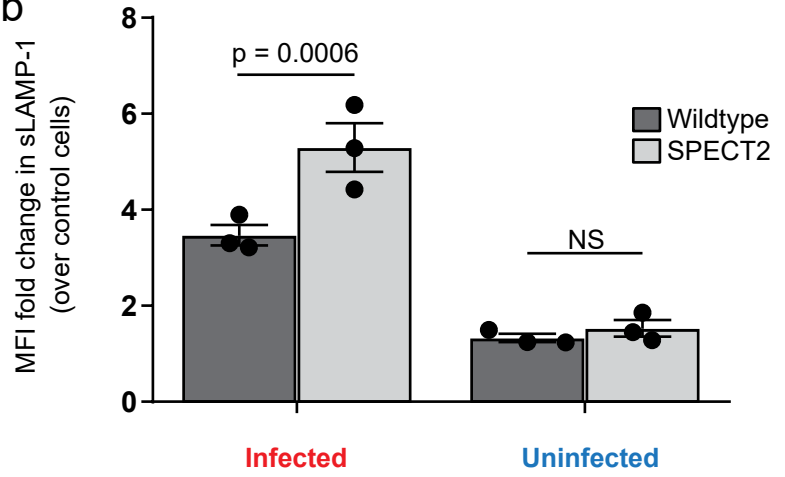
169

170

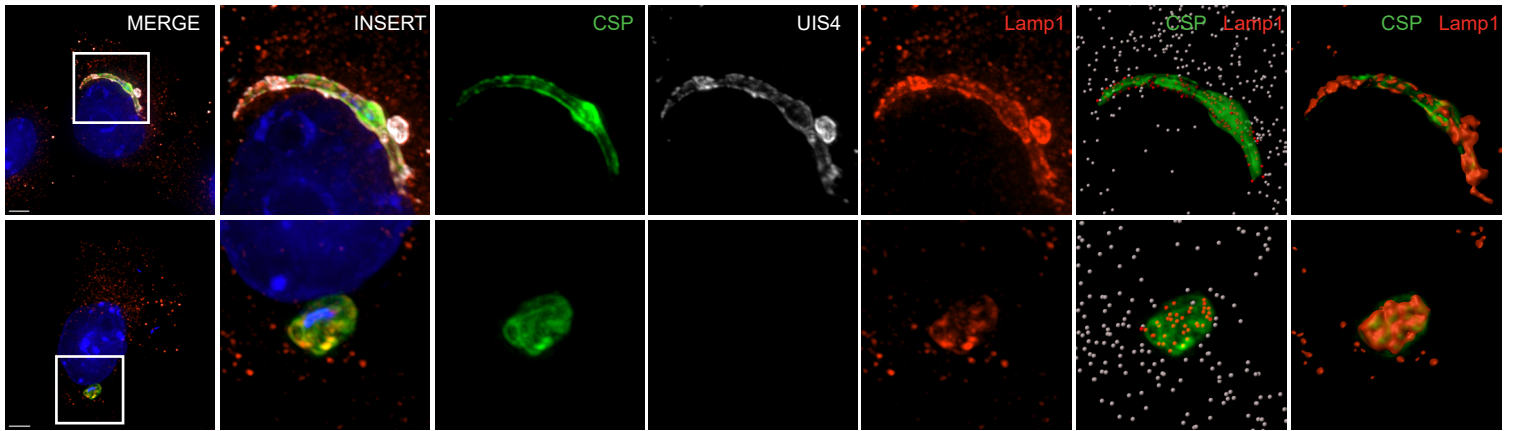
a



b



c



171 **Fig. S3. Sporozoite induced lysosome-plasma membrane fusion is independent of productive**  
172 **invasion. (a)** Hepa1-6 cells were infected with SPECT2<sup>-</sup> *P. yoelii* sporozoites for 90 min and  
173 analyzed by flow cytometry using antibodies specific to LAMP1 and CSP. Surface LAMP1 was  
174 evaluated by staining cells prior to permeabilization, while total LAMP1 was evaluated by staining  
175 for LAMP1 after permeabilization. The histogram shows the distribution of surface LAMP1 from  
176 SPECT2<sup>-</sup> infected, uninfected and unexposed control cells from one of three independent  
177 experiments. **(b)** Surface LAMP1 levels were compared between uninfected and SPECT2<sup>-</sup> infected  
178 cells as a fold change over control cells. The bar graph depicts the mean  $\pm$  the SD of three  
179 independent experiments. **(c)** Hepa1-6 cells were infected with *P. yoelii* sporozoites and fixed after  
180 90 min. Cells were stained with DAPI (blue) for nuclei visualization, antibodies to LAMP1 for  
181 lysosomes, UIS4 (white) and CSP (green) for parasite detection and displayed as maximum  
182 intensity projections. Bar = 5  $\mu$ m. Red spots represent LAMP1-positive structures co-localized  
183 with CSP. Magnified inset is 15  $\mu$ m x 15  $\mu$ m. Related to Figure 2.

184

185

186

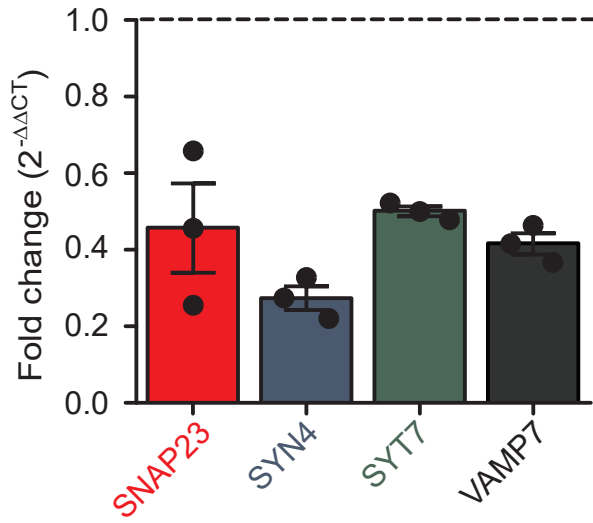
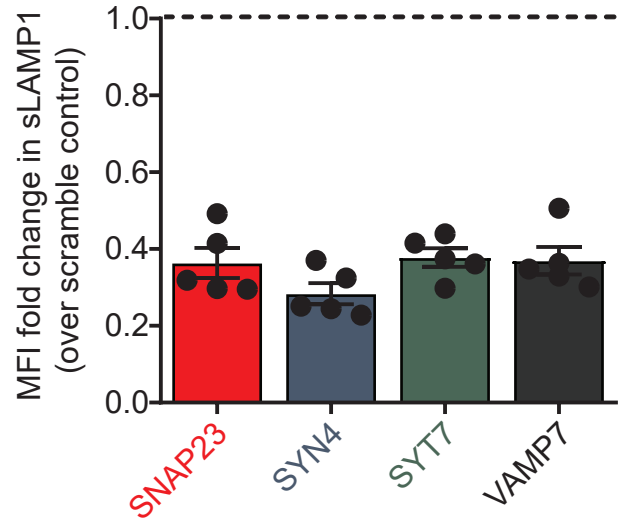
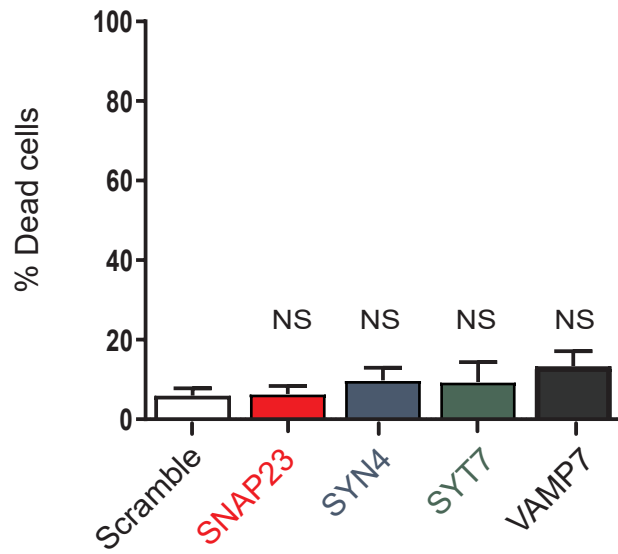
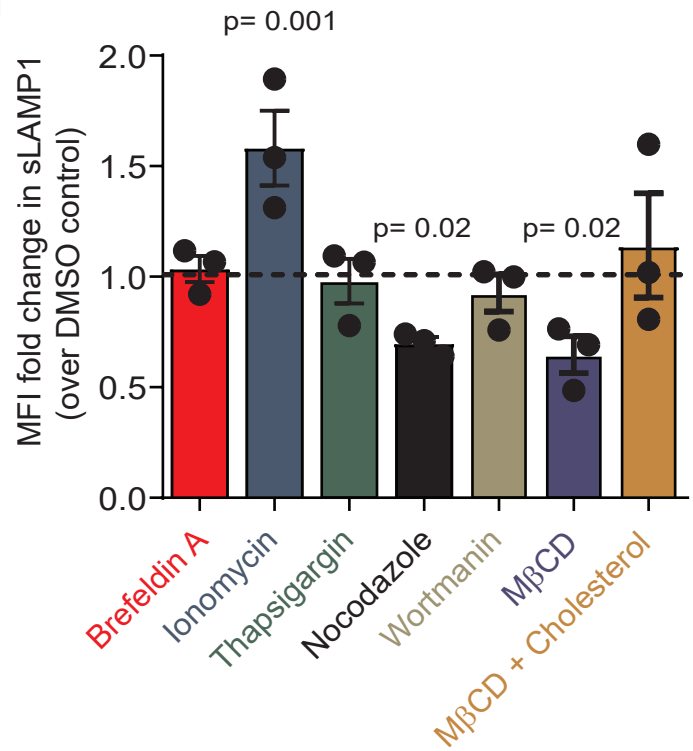
187

188

189

190

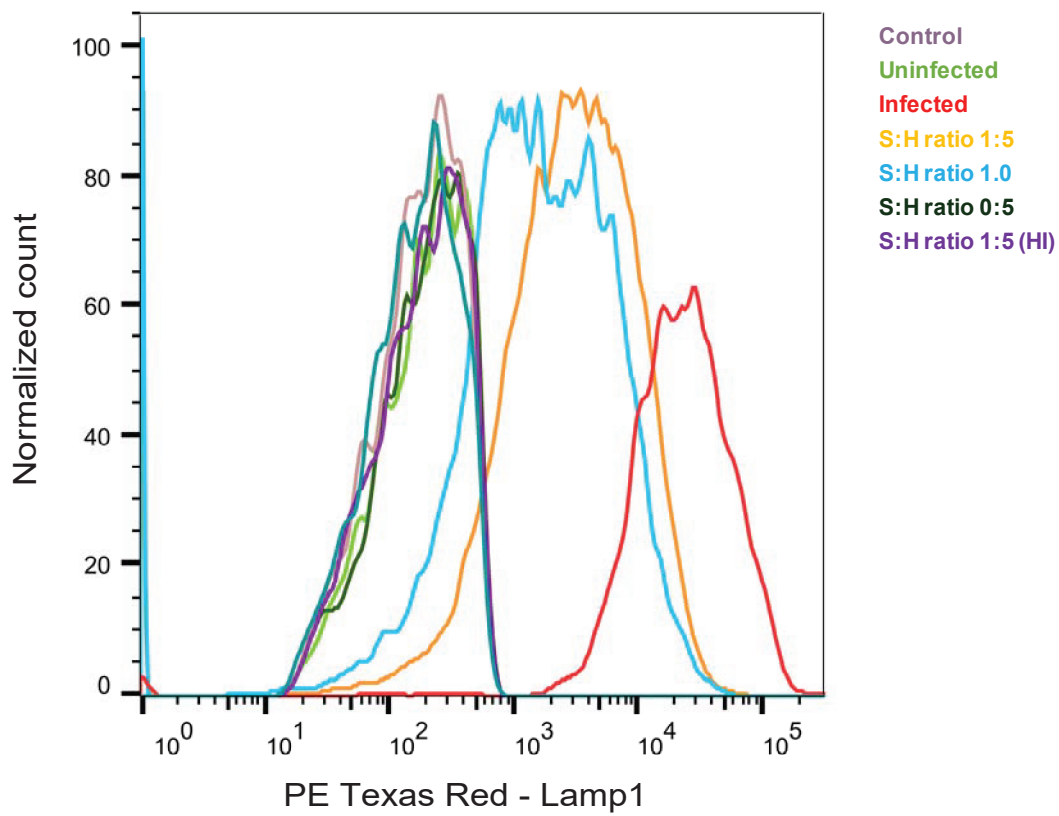
191

**a****b****c****d**

192 **Fig. S4. Selective knockdown of SNARE proteins can be achieved using lentivirus-mediated**  
193 **shRNA. (a)** Bar graph depicting relative gene knockdown compared to non-targeting control  
194 shRNA. Hepa 1-6 cells were transduced with lentivirus expressing shRNA constructs selectively  
195 targeting SNARE proteins, or a non-targeting control. Mean knockdown level was determined  
196 using qPCR. Values are normalized to non-targeting control which is indicated by solid black line.  
197 Data is mean  $\pm$  the SD of 3 independent experiments. **(b)** Hepa1-6 cells were transduced with  
198 shRNA lentiviruses against SNAP23, SYN4, SYT7, or VAMP7 or a scrambled control and  
199 assessed for surface LAMP1 by flow cytometry. Surface LAMP1 levels were compared between  
200 scramble and specific knockdowns and expressed as a fold change in mean fluorescent intensity  
201 (MFI). The bar graph depicts the mean  $\pm$  the SD of 5 independent experiments. **(c)** Hepa1-6 cells  
202 were transduced with shRNA lentiviruses against SNAP23, SYN4, SYT7, VAMP7 or a scrambled  
203 control and challenged with *P. yoelii* sporozoites for 90 min and stained with Live/Dead stain for  
204 30 mins before fixation. The bar graph displays the dead cell percentage in knockdowns  
205 normalized to scramble shRNA cells, indicated by dashed line following infection. **(d)** Hepa1-6  
206 cells were incubated with or without 10  $\mu$ M ionomycin, 400 nM thapsigargin, 10  $\mu$ M brefeldin A,  
207 10  $\mu$ M nocodazole, 5 mM methyl- $\beta$ -cyclodextrin (M $\beta$ CD) for 15 min, fixed and assessed for  
208 surface LAMP1 by flow cytometry. For cholesterol replenishment, methyl- $\beta$ -cyclodextrin  
209 (M $\beta$ CD) treated cells were incubated with 1 mM cholesterol for 15 min prior to fixation. Surface  
210 LAMP1 levels were compared between DMSO vehicle control and specific treatments and  
211 expressed as a fold change in mean fluorescent intensity (MFI). The bar graph depicts the mean  $\pm$   
212 the SD of three independent experiments. Related to Figure 3.

213

214

**a**

215 **Fig. S5. Sporozoite secreted factor(s) contribute to relocalisation of lysosomes.** Hepa1-6 cells  
216 were infected with *P. yoelii* sporozoites or exposed to sporozoite secretion-enriched supernatants.  
217 Surface LAMP1 was analyzed by flow cytometry. Histogram is representative of three  
218 independent experiments. Related to Figure 4.

219

220

221

222

223

224

225

226

227

228

229

230

231

232

233

234

235

236

237

238

239 **Supplementary Table 1**

240 Lysosomal trafficking modulators selected for the study. Related to Figure 3

Inhibitor	Function	Reference
Ionomycin	ionophore, increases intracellular Ca <sup>++</sup> and induces lysosome exocytosis.	(Xu et al., 2012)
Brefeldin A	redistributes LE/lysosomes towards periphery	(Lippincott-Schwartz et al., 1991; Tardieux et al., 1992)
Nocodazole	a microtubule-depolymerizing agent, prevents lysosome redistribution.	(Tardieux et al., 1992)
Thapsigargin	inhibitor of the sarco/endoplasmic reticulum Ca <sup>++</sup> ATPase, elevates cytosolic Ca <sup>++</sup> and promotes lysosome exocytosis.	(Sivaramakrishnan et al., 2012)
Methyl- $\beta$ -cyclodextrin	depletes membrane cholesterol and reduces LAMP1 levels on surface.	(Hissa et al., 2012)
Wortmannin	PI3K inhibitor, inhibits various stages of endocytic network.	(Sinnberg et al., 2009)

241

242

243

244

245

246

247

248

249

250

251 **References:**

252

- Hissa, B., Duarte, J.G., Kelles, L.F., Santos, F.P., del Puerto, H.L., Gazzinelli-Guimaraes, P.H., de Paula, A.M., Agero, U., Mesquita, O.N., Guatimosim, C., *et al.* (2012). Membrane cholesterol regulates lysosome-plasma membrane fusion events and modulates *Trypanosoma cruzi* invasion of host cells. *PLoS neglected tropical diseases* *6*, e1583.
- Lippincott-Schwartz, J., Yuan, L., Tipper, C., Amherdt, M., Orci, L., and Klausner, R.D. (1991). Brefeldin A's effects on endosomes, lysosomes, and the TGN suggest a general mechanism for regulating organelle structure and membrane traffic. *Cell* *67*, 601-616.
- Real, F., and Mortara, R.A. (2012). The diverse and dynamic nature of *Leishmania* parasitophorous vacuoles studied by multidimensional imaging. *PLoS neglected tropical diseases* *6*, e1518.
- Schenkman, S., Jiang, M.S., Hart, G.W., and Nussenzweig, V. (1991). A novel cell surface trans-sialidase of *Trypanosoma cruzi* generates a stage-specific epitope required for invasion of mammalian cells. *Cell* *65*, 1117-1125.
- Sinnberg, T., Lasithiotakis, K., Niessner, H., Schitteck, B., Flaherty, K.T., Kulms, D., Maczey, E., Campos, M., Gogel, J., Garbe, C., *et al.* (2009). Inhibition of PI3K-AKT-mTOR signaling sensitizes melanoma cells to cisplatin and temozolomide. *J Invest Dermatol* *129*, 1500-1515.
- Sivaramakrishnan, V., Bidula, S., Campwala, H., Katikaneni, D., and Fountain, S.J. (2012). Constitutive lysosome exocytosis releases ATP and engages P2Y receptors in human monocytes. *Journal of cell science* *125*, 4567-4575.
- Tardieux, I., Webster, P., Ravesloot, J., Boron, W., Lunn, J.A., Heuser, J.E., and Andrews, N.W. (1992). Lysosome recruitment and fusion are early events required for trypanosome invasion of mammalian cells. *Cell* *71*, 1117-1130.
- Xu, J., Toops, K.A., Diaz, F., Carvajal-Gonzalez, J.M., Gravotta, D., Mazzoni, F., Schreiner, R., Rodriguez-Boulan, E., and Lakkaraju, A. (2012). Mechanism of polarized lysosome exocytosis in epithelial cells. *Journal of cell science* *125*, 5937-5943.